



HAL
open science

Anisotropic thermal conductivity of natural Boom Clay

Linh Quyen Dao, Pierre Delage, Anh Minh A.M. Tang, Yu-Jun Cui,
Jean-Michel Pereira, Xiang-Ling Li, Xavier Sillen

► **To cite this version:**

Linh Quyen Dao, Pierre Delage, Anh Minh A.M. Tang, Yu-Jun Cui, Jean-Michel Pereira, et al..
Anisotropic thermal conductivity of natural Boom Clay. *Applied Clay Science*, 2014, 101, pp.282-287.
hal-01111299

HAL Id: hal-01111299

<https://enpc.hal.science/hal-01111299v1>

Submitted on 26 Apr 2018

HAL is a multi-disciplinary open access archive for the deposit and dissemination of scientific research documents, whether they are published or not. The documents may come from teaching and research institutions in France or abroad, or from public or private research centers.

L'archive ouverte pluridisciplinaire **HAL**, est destinée au dépôt et à la diffusion de documents scientifiques de niveau recherche, publiés ou non, émanant des établissements d'enseignement et de recherche français ou étrangers, des laboratoires publics ou privés.

Anisotropic thermal conductivity of natural Boom Clay

Linh-Quyen DAO¹, Pierre DELAGE¹, Anh-Minh TANG¹, Yu-Jun CUI¹

Jean-Michel PEREIRA¹, Xiang-Ling LI², Xavier SILLEN³

¹ Ecole des Ponts ParisTech, UR Navier/CERMES, 6-8, av. Blaise Pascal, Cité Descartes, 77455 Marne-la-Vallée, France.

² European Underground Research Infrastructure for Disposal of nuclear waste in Clay Environment (EURIDICE, Mol, Belgium)

³ Belgian Agency for Radioactive Waste and Enriched Fissile Materials (ONDRAF/NIRAS, Brussels, Belgium)

Corresponding author:

Prof. Yu-Jun CUI

Ecole des Ponts ParisTech

6-8 av. Blaise Pascal, Cité Descartes, Champs-sur-Marne

77455 Marne-la-Vallée cedex 2

France

Email : yujun.cui@enpc.fr

Phone : +33 1 64 15 35 50

Fax : +33 1 64 15 35 62

31 **Abstract**

32 The thermal conductivity of host rocks is an important parameter in the design of deep geological
33 disposal of heat-emitting radioactive waste. Due to bedding, heat transfer in sedimentary rocks is
34 affected by their transversally isotropic structure. In this work, an experimental program is run to
35 measure the thermal conductivities of Boom Clay along various orientations with respect to the
36 bedding plane by using the needle thermal probe technique. Measurements were performed on
37 specimens obtained from cores drilled from the HADES Underground Research Laboratory (URL) at
38 Mol, Belgium, at a depth of 223 m. The thermal conductivities values obtained are in good agreement
39 with those previously published, confirming the thermal anisotropy of the Boom Clay. Moreover, the
40 observed changes in thermal conductivity with respect to the distance to the gallery provide further
41 evidence on the extent of the Excavation Damaged Zone around the gallery.

42

43 **Keywords:** Thermal conductivity; Boom Clay; thermal anisotropy; excavation damaged zone;
44 laboratory test.

45

46

47

48

49

50

51

52

53

54

55

56 **1 Introduction**

57 In the context of deep geological disposal of heat-emitting high activity radioactive waste, the thermal
58 conductivity of the host geological formation (stiff clays, mudstones, granites, etc.) is an important

59 parameter in the design of the disposal. Moreover, the thermal transient phase that will be experienced
60 by the system over hundreds to thousands of years after waste emplacement represents an important
61 part of its long-term evolution (Yu et al., 2013). Due to a layered microstructure resulting from the
62 initial deposition and further geological processes, stiff clays and claystones are known to
63 preferentially conduct heat along the direction parallel to the bedding plane. Indeed, this anisotropy of
64 thermal conductivity was observed in various stiff clays and claystones including the London clay, the
65 Callovo-Oxfordian claystone (COx, East of France) and the Opalinus clay (Switzerland). In London
66 clay, the thermal conductivity in the direction perpendicular to the bedding plane was found equal to
67 0.83 W/(m.K) whereas that in the direction parallel to the bedding plane was equal to 1.19 W/(m.K)
68 (Midttømme and Roaldset, 1999). The thermal conductivity of Opalinus Clay was investigated by
69 Mügler et al. (2006). They reported that the values obtained by in-situ back analysis are 0.55 - 1.07
70 W/(m.K) in the direction perpendicular to bedding and 1.84 - 1.90 W/(m.K) in the direction parallel to
71 bedding, respectively. Buntebarth (2004) (in Jobmann and Polster, 2007) gave, from laboratory
72 experiments, thermal conductivities of 0.75 W/(m.K) and 1.55 W/(m.K) for the directions
73 perpendicular and parallel to bedding, respectively. The thermal conductivity in the direction
74 perpendicular to the bedding plane of the COx claystone varies between 1.3 and 1.9 W/(m.K) whereas
75 that in the direction parallel to the bedding plane varies between 1.9 and 2.7 W/(m.K) (ANDRA,
76 2005).

77 Based on the values in the two directions, a degree of thermal conductivity anisotropy (or anisotropy
78 effect) η can be defined, as follows (Popov et al., 1999; Pribnow et al., 2000; Davis et al., 2007):

$$\eta = \frac{\lambda_{//}}{\lambda_{\perp}} \quad (1)$$

79 From the values of thermal conductivity introduced above, a value of $\eta = 1.43$ is determined for
80 London clay. For Opalinus Clay and COx claystone, η can vary from 1.78 to 3.34 and from 1.42 to
81 1.46, respectively.

82 In Boom Clay, the anisotropy of thermal conductivity has been inferred through the back analysis of a
83 small scale in-situ heating experiment, ATLAS III, carried out in the Underground Research
84 Laboratory (URL) HADES at a depth of 223 m (Chen et al., 2011). The measurements of temperature
85 evolution at different distances from the heater were compared with the results of heat transfer

86 simulations. In those simulations, adopting values of thermal conductivities equal to 1.65 W/(m.K)
87 and 1.31 W/(m.K) for the directions parallel and perpendicular to the bedding plane, respectively, led
88 to good agreement with the measured temperatures. It is worth noting that, in some sedimentary
89 rocks, the thermal conductivity in the direction parallel to the bedding plane is more than twice higher
90 than that in the direction perpendicular to the bedding plane (Midttømme et al., 1996). After Schön
91 (1996), the reasons for this anisotropy in thermal conductivity of sedimentary rocks are: (i) crystal
92 anisotropy of the individual rock-forming minerals; (ii) intrinsic or structural anisotropy resulting from
93 the mineral shapes and their textural arrangement within the rock; (iii) orientation and geometry of
94 crack fractures and other defects. Point (ii) is particularly true in the case of clays and claystones
95 because of the planar shape of clay platelets and the bedding orientation by long term consolidation,
96 creep and diagenesis.

97

98 In addition to anisotropy, the presence of the Excavation Damage Zone (EDZ) around underground
99 constructions can also influence the thermal conductivity. However, few studies have been devoted to
100 this aspect.

101

102 Three methods are often used to measure the thermal conductivity of soils in the laboratory: i) the
103 divided bar method, ii) the needle probe method (or line source method) and iii) optical scanning. The
104 divided bar method is a steady state method in which a constant temperature gradient is imposed
105 across the sample, resulting in a stable heat flow. This method involves heat transmission along a
106 single direction only, and is considered to be accurate (Johansen, 1975; Farouki, 1981; Brigaud et al.,
107 1990; Midttømme and Roaldset, 1999). It is also recommended to be used in measuring the thermal
108 conductivity of rock samples (Beck, 1988; Ashworth, 1990). The needle probe method is a transient
109 method in which a radial heat flow is produced within the specimen while measuring temperature
110 changes over time. This method is based on the theory of axisymmetric heat diffusion from an infinite
111 line source within an infinite surrounding medium. It is valid when the ratio between the length and
112 the diameter of the needle is larger than 30:1 (Popov et al., 1999). The thermal conductivity can hence
113 be back calculated from the temperature-time curve (Jessop, 1990). In the optical method (Popov,
114 1983), a focused, mobile and continuously operated heat source is used to heat a sample while

115 monitoring temperature changes using infrared temperature sensors. The excess temperatures
116 monitored on the sample are compared to that of a reference sample of known thermal conductivity,
117 allowing the thermal conductivity to be determined. This method has been recommended to estimate
118 the thermal anisotropy of rocks (Popov et al., 1999).

119

120 In this paper, the needle probe method was selected for its simplicity and standardisation. The thermal
121 anisotropy of Boom Clay was investigated by adopting various orientations of the needle with respect
122 to the bedding orientation of the samples. These experimental results were then compared with the
123 theoretical results. The Boom Clay samples were extracted from a series of cores taken from a
124 horizontal borehole drilled from a gallery of the HADES URL. The core was at 2.40 m to 22.3 m
125 distance to the gallery axis (HADES borehole 2012-2 / Connecting Gallery / Ring 66-67W) and the
126 specimens were extracted from the core at various distances ranging from 2.5 to 20.8 m to the gallery
127 axis.

128

129 **2 Background**

130 **2.1 Anisotropy of thermal conductivity**

131 Heat flow by conduction along one dimension is governed by Fourier's law:

$$q = -\lambda \frac{dT}{dx} \quad (2)$$

132 where q is the heat flux density (W/m^2), λ is the thermal conductivity ($\text{W}/(\text{m}\cdot\text{K})$) and dT/dx is the
133 temperature gradient along the x direction.

134 In an anisotropic material, the apparent thermal conductivity λ measured on an anisotropic sample
135 around a line-source is related to the principal components of the thermal conductivity tensor (Grubbe
136 et al., 1983; Popov et al., 1999), as follows:

$$\lambda = \sqrt{\lambda_A \lambda_B \cos^2(\gamma) + \lambda_A \lambda_C \cos^2(\beta) + \lambda_B \lambda_C \cos^2(\alpha)} \quad (3)$$

137 where, λ_A , λ_B and λ_C are the three principal components of the thermal conductivity tensor; α , β and γ
138 are the angles between the line-source axis and the principal directions of thermal conductivity tensor

139 A, B and C, respectively (Fig. 1). Knowing the angles α , β and γ in equation (3), the apparent thermal
 140 conductivity λ can be determined through three measurements.

141 Due to the stratification and bedding, many sedimentary rocks and clays are transversely isotropic,
 142 leading to the following relations: $\lambda_A = \lambda_{\perp}$ (thermal conductivity in the direction perpendicular to the
 143 bedding plane) and $\lambda_B = \lambda_C = \lambda_{//}$ (thermal conductivity in the direction parallel to the bedding plane). If
 144 the axis of the emitting needle probe is perpendicular to the bedding plane (Fig. 1a), $\alpha = 0^\circ$ and $\beta = \gamma$
 145 $= 90^\circ$. Hence:

$$\lambda_0 = \sqrt{\lambda_B \lambda_C \cos^2(0^\circ)} = \lambda_{//} \quad (4)$$

146 When the needle is parallel to the bedding plane (Fig. 1b), $\alpha = \gamma = 90^\circ$, $\beta = 0^\circ$ and λ represents λ_{90} :

$$\lambda_{90} = \sqrt{\lambda_A \lambda_C \cos^2(0^\circ)} = \sqrt{\lambda_{\perp} \lambda_{//}} \quad (5)$$

147 From (4) and (5):

$$\lambda_{\perp} = \frac{(\lambda_{90})^2}{\lambda_0} \quad (6)$$

148 Equation (6) has been used by several authors (Penner, 1963; Munroe and Sass, 1987; Popov et al.,
 149 1999; Pribnow et al., 2000; Gong, 2005; Davis et al., 2007; Popov et al., 2012; Riche and Schneebeil,
 150 2012) to determine the value of thermal conductivity in the direction perpendicular to bedding λ_{\perp}
 151 based on the measurements of λ_{90} and λ_0 in different materials (clay sediments, igneous rocks, snow,
 152 etc.).

153

154 In general, when the line source axis forms an angle θ with the normal to the bedding (Fig. 1c), an
 155 apparent thermal conductivity can be determined by:

$$\lambda_{\theta} = \sqrt{\lambda_{\perp} \lambda_{//} \sin^2(\theta) + (\lambda_{//})^2 \cos^2(\theta)} \quad (7)$$

156 Thus,

$$\lambda_{\theta} = \sqrt{(\lambda_0)^2 \cos^2(\theta) + (\lambda_{90})^2 \sin^2(\theta)} \quad (8)$$

157 Equation (8) was firstly proposed by Pribnow (cited by Davis et al., 2007). This function was used to
 158 compare the experimental results with the changes in probe orientation. The data of Davis et al. (2007)
 159 agree reasonably well with equation (8).

160 To calculate the value for $\theta = 45^\circ$, substituting equation (6) into equation (8) yields:

$$\lambda_{45} = \sqrt{\frac{(\lambda_0)^2 + (\lambda_{90})^2}{2}} \quad (9)$$

161

162 **2.2 Thermal conductivity at saturated state**

163 Various authors stated that the thermal conductivity of clays depends on several factors such as the
164 composition (solid, water and gas phases), the nature of the dominant minerals, the density/porosity,
165 the temperature, etc. (Farouki, 1986; Clauser and Huenges, 1995; Midttømme and Roaldset, 1999;
166 Tang et al., 2008). In this study, the effects of the slight changes in degree of saturation (S_r) and
167 density of the investigated samples were taken into account based on the Johansen's method (Farouki,
168 1986). According to Johansen, the thermal conductivity of an unsaturated soil is a function of its
169 thermal conductivity at dry and saturated states at the same dry density. To establish this function,
170 Johansen (1975) introduced a normalized thermal conductivity, namely Kersten's number (K_e):

$$K_e = (\lambda - \lambda_{dry}) / (\lambda_{sat} - \lambda_{dry}) \quad (10)$$

171 where λ_{sat} is the thermal conductivity at saturated state, λ is the thermal conductivity at intermediate
172 degree of saturation, λ_{dry} is the thermal conductivity at dry state

173 Hence, one can deduce the saturated thermal conductivity value from the thermal conductivity
174 measurement conducted on non-saturated samples, according to the following relationship:

$$\lambda_{sat} = \frac{(\lambda - \lambda_{dry})}{K_e} + \lambda_{dry} \quad (11)$$

175 In fine-grained unfrozen soils, Johansen proposes the following relationships for K_e and λ_{dry} :

$$K_e \cong \log S_r + 1.0 \quad (12)$$

176

$$\lambda_{dry} = \frac{0.135\rho_d + 64.7}{2700 - 0.947\rho_d} \pm 20\% \text{ (W / (m.K))} \quad (13)$$

177 where ρ_d is the dry density in kg/m^3 .

178 **3 Material and methods**

179 **3.1 The Boom Clay**

180 In Belgium, researches on geological radioactive waste disposal in clay formation were initiated by
181 SCK•CEN in 1974. The first Underground Research Laboratory (URL) HADES was then excavated
182 in Boom Clay formation at a depth of 223 m during the early Eighties at a site close to the city of Mol
183 and has been progressively extended since. The Boom Clay was chosen as a potential host rock for
184 radioactive waste disposal due to its very low permeability (its hydraulic conductivity around $2 \cdot 10^{-12}$
185 m/s and $5 \cdot 10^{-12}$ m/s in the direction perpendicular and parallel to the bedding, respectively), its
186 capacity to retard the migration of many radionuclides by sorption, its high plasticity, and its capacity
187 of self-sealing after physical disturbances.

188

189 Located at 190 m - 290 m below ground level at Mol (ONDRAF/NIRAS, 2001), Boom Clay was
190 deposited during the Tertiary Era about 30 millions years ago. The Boom Clay layer is almost
191 horizontal with a slight 1-2% north-east dip. It is located between water-bearing sand layers
192 (ONDRAF/NIRAS, 2001).

193

194 In order to investigate both the anisotropy in thermal conductivity of Boom Clay and the possible
195 influence of the excavation damaged zone (EDZ) on it, nine samples were taken at various distances
196 from the gallery (4.0 m in diameter, 0.4 m in liner thickness) from the core (100 mm in diameter)
197 taken from a borehole (reference number: R66-67/2012) drilled horizontally till approximately 22 m in
198 length, in July 2012. Once drilled, the core was immediately sealed under vacuum in aluminium foils
199 to minimize drying effects. Table 1 summarizes the physical properties of the nine samples. The
200 distance to the gallery axis r varies from 2.5 m to 20.8 m. The water content of the samples (w)
201 slightly changes from 22.6% to 24%, which is in the range of the in-situ measurements (from 22% to
202 27%). The densities are comparable (1630 - 1640 kg/m³) except for the sample that was the closest to
203 the gallery (TH6, $r = 2.9$ m, $\rho_d = 1.61$ Mg/m³). A suction measurement was made on sample TH11 (r
204 = 9.60 m) using a chilled mirror hygrometer (WP4, Decagon Device), and a value of 2.8 MPa was

205 obtained, in good agreement with the suction value reported in Delage et al. (2007) from a sample at
206 the same depth.

207

208 **3.2 Thermal conductivity measurements**

209 The apparatus used to measure the thermal conductivity is a commercial handheld device named KD2
210 Pro Thermal Properties Analyzer (Decagon Devices, Inc.). The kit consists of a controller and 3
211 separated sensors (small single needle, large single needle, dual needle) that can be inserted into the
212 tested medium. The small single needle (60 mm in length, 1.3 mm in diameter) (Fig. 2b) was used to
213 measure the thermal conductivity of Boom Clay. The accuracy of the thermal conductivity
214 measurement using this needle is $\pm 5\%$ from 0.2 W/(m.K) - 2 W/(m.K).

215

216 Cylindrical samples were trimmed from cores (100 mm in diameter and 60mm - 90 mm in height).
217 The bedding orientation that could be identified from direct visual observation was marked. The
218 samples were then slightly confined by means of an adhesive tape so as to avoid further crack
219 propagation and any perturbation.

220

221 Three holes were prepared in each sample by drilled in each sample using a drilling-machine (Fig. 2a)
222 equipped with a thin steel drill (1.3 mm in diameter, 65 mm in effective length). In order to ensure a
223 good thermal contact between specimen and probe, the needle probe was coated with a thin layer of
224 thermal grease (high-density polysynthetic silver thermal compound by Arctic Silver) prior to its
225 insertion into the drilled hole (Fig. 2b), as recommended by the ASTM standard D5334-08 (2008). For
226 a better precision, it was decided to run 5 successive measurements at intervals of 15 minutes.

227

228 The measured thermal conductivity values were denoted λ_0 , λ_{45} and λ_{90} , defined by the value of the
229 angle θ between the axis of the hole and the direction normal to the bedding (see Fig. 1 and Fig. 3). As
230 mentioned previously, heat transfer in the case of $\theta = 0^\circ$ is parallel to the bedding (Fig. 1a), and the λ_0
231 value measured by the needle device is equal to the thermal conductivity in the direction parallel to the
232 bedding ($\lambda_{//}$). In the two other cases, the measured values depend on the thermal conductivities in the

233 directions parallel and perpendicular to the bedding. The thermal conductivity in the direction
234 perpendicular to the bedding (λ_{\perp}) needs to be back calculated, as seen in the previous section.

235

236 **4 Experimental results**

237 **4.1 Anisotropy of thermal conductivity**

238 Since the degrees of saturation of the nine specimens are slightly lower than 100% (see Table 1), the
239 thermal conductivities at saturated state were first calculated using equation (11). As seen in Table 2 in
240 which the initial ($\lambda_{i/0}$) and corrected $\lambda_{i/}$ values are presented, the corrections made for saturation are
241 small with a relative variation ($\Delta\lambda_{i/} / \lambda_{i/0}$) included between 0.64% and 2.04%. The values of thermal
242 conductivity in the direction perpendicular to the bedding at saturated state λ_{\perp} were afterwards
243 determined using equation (6) based on the value of λ_{90} determined from a test with the needle parallel
244 to the bedding (Fig. 3). The thermal conductivity anisotropy ratio η was then deduced from equation

245 **Erreur ! Source du renvoi introuvable..**

246

247 **4.2 Influence of EDZ on thermal conductivity**

248 The changes in thermal conductivity along the three directions (λ_0 , λ_{45} , λ_{90} , Fig. 3) with respect to the
249 distance to the gallery axis r are shown in Fig. 4. The gallery wall is also represented in this figure.
250 The vertical bars indicate the range of the 5 measurements performed on each sample. The calculated
251 values of λ_{45} (from λ_0 and λ_{90} using equation (9)) are also plotted for comparison with the test data
252 directly obtained using the needle probe inclined at 45° with respect to the bedding. Excellent
253 agreement was observed, confirming: (i) 2D anisotropy model (presented in the part 2.1), (ii)
254 correspondence of principal axes of thermal conductivity to bedding plane orientation shown in Figure
255 1.

256 Fig. 4 shows that all the measurements start from a low value in the zone close to the gallery wall
257 (around 1.3 W/(m.K) for $\lambda_0 = \lambda_{i/}$ at $r = 2.5$ m). The conductivity values increase with distance to reach
258 a maximum value at around 6.4 m from the gallery axis (1.6 W/(m.K) for $\lambda_{i/}$). A slight decrease ($\lambda_{i/}$) or
259 a more significant one (λ_{\perp}) is observed for samples taken at greater distances from the gallery (up to

260 20.8 m). The average value of 1.6 W/(m.K) for $\lambda_{//}$ observed at larger distances is in good agreement
261 with the value of 1.65 W/(m.K) obtained from the back calculations carried out within the ATLAS III
262 project (Chen et al., 2011; Yu et al., 2011).

263

264 These results also confirm that the thermal conductivity in the direction parallel to the bedding is
265 always higher than that in the direction perpendicular to the bedding. The values of $\lambda_{//}$ vary between
266 1.34 - 1.61 W/(m.K) whereas those of λ_{\perp} vary between 0.82 – 1.06 W/(m.K) (Fig. 4). This can also be
267 observed in Fig. 5 that presents the changes in anisotropy ratios η versus the distance r to the gallery
268 axis. The values of η change between 1.5 and 1.8 with no significant effect of the distance to the
269 gallery axis. Note that the value of λ_{\perp} obtained in this study is smaller than that obtained by back
270 calculations (1.31 W/(m.K)) by Chen et al. (2011). This difference may be explained by the fact that
271 λ_{\perp} is much more dependent on confinement (that strongly affects the contact between parallel clay
272 particles) than $\lambda_{//}$. Further studies on the effect of confinement on the anisotropic thermal conductivity
273 are needed to confirm this point.

274

275 **5 Discussion**

276 It is now well recognized that an Excavation Damaged Zone (EDZ) characterized by a fracture
277 network including shear and tension fractures along with a herringbone pattern of fractures develops
278 during excavation in clays and claystones (Mertens et al., 2004; Bastiaens and Mertens, 2005; Davies
279 and Bernier, 2005; Tsang et al., 2005; Bernier et al., 2007; Tsang et al., 2012; Armand et al., 2013).
280 The extent of this zone depends on various parameters such as the nature of the media (soft clay, stiff
281 clay or claystone), its mechanical properties, the excavation technique, the state of stress around the
282 gallery and the bedding orientation. Around the Connecting Gallery of the URL HADES at Mol, an
283 EDZ characterized by a herringbone fracture pattern has been observed (Bastiaens and Mertens, 2005;
284 Bernier et al., 2007) with open fractures extending to about 1 m from the gallery wall. There were
285 indications that the extent in the horizontal direction was somewhat larger than in the vertical
286 direction.

287

288 The thermal conductivity measurements carried out in this study on samples extracted from a
289 horizontal borehole at various distances from the gallery axis evidenced changes that can be related to
290 the EDZ, given that discontinuities are suspected to affect heat transfer across these. In this regard, the
291 thermal conductivity changes in the direction parallel to the bedding ($\lambda_{//}$) seems to be the more
292 significant parameter to be considered since the borehole was horizontal with a sub-vertical orientation
293 of cracks in this area. Indeed, inspection of Fig. 4 shows that parameter $\lambda_{//}$ starts from small values to
294 afterwards increase with the distance to the gallery (until a distance r of 4.0 m from the gallery axis,
295 corresponding to about 1.6 m from the outside wall). Beyond this distance, the horizontal thermal
296 conductivity remains about constant, around a value of 1.6 W/(m.K), in good accordance with the
297 back analysis of the in-situ heating test. Based on the thermal conductivity measurements, it is
298 deduced that the EDZ extension in the horizontal direction is about 1.6 m from the outside of gallery's
299 wall, a value in consistence with in situ observation.

300

301 The data presented here were obtained from the laboratory measurements carried out on samples
302 extracted from a horizontal core and under zero confining stress. As a result, there would be some
303 possibility of cracks' opening within the samples due to stress release. Thereby, the effects of cracks
304 on thermal fluxes observed in Fig. 4 could be enhanced by the stress release. Thus, the question arises
305 as to whether the changes in thermal conductivity with respect to the distance to the gallery really
306 occur in-situ. Actually, clays are known to exhibit self-sealing properties with respect to water
307 transfer. This self-sealing behaviour, interpreted as the recovery of a good contact between the two
308 faces of discontinuities, could have comparable consequence on heat transfer as well. In other words,
309 self-sealing could be extended from fluid transfer to heat transfer. Such a hypothesis should obviously
310 be further investigated by thermal conductivity measurements in the laboratory, under confining
311 conditions and/or running detailed in-situ measurement at various distances from the gallery
312 completed by thermal back-analysis of in-situ thermal tests. Meanwhile, the changes in thermal
313 conductivity carried out here on laboratory samples provide a complementary identification of the
314 extent of the EDZ along a horizontal direction around the gallery excavated in Boom Clay.

315

316 **6 Conclusion**

317 An experimental study using the needle thermal probe technique was conducted for investigating the
318 thermal conductivity anisotropy of natural Boom Clay. The investigation was carried out on samples
319 extracted from a series of cores (from a single borehole) taken from the Underground Research
320 Laboratory at Mol in Belgium, at a depth of 223 m. Thermal conductivity was measured on specimens
321 sampled at various distances to the gallery axis, from 2.5 to 20.8 m. Measurements were conducted
322 along three directions: parallel, perpendicular and at an angle of 45° with respect to the bedding plane.
323 A significant thermal anisotropy was evidenced and data confirmed that the highest conductivity was
324 in the direction parallel to bedding and that the smallest one was in the direction perpendicular to
325 bedding, the one at 45° being logically in between these two values. It is worth noting that the
326 conductivity values found in this laboratory study in the direction parallel to the bedding was close to
327 that back-calculated from the in-situ ATLAS experiments (Chen et al., 2011).

328 The effect of an excavation damaged zone (EDZ) was also evidenced: the thermal conductivity in the
329 three directions increased with the distance to the gallery. Based on the experimental data, an EDZ
330 extent of about 1.6 m in the horizontal direction was identified, a value consistent with the in situ
331 observation. Finally, the thermal anisotropy did not appear to be significantly affected by the
332 excavation damage, with no significant effect of the distance to the gallery on the thermal anisotropy
333 ratio that was comprised between 1.48 and 1.74.

334

335 **Acknowledgements**

336 The authors are grateful to Ecole des Ponts ParisTech (ENPC), the European Underground Research
337 Infrastructure for Disposal of nuclear waste In Clay Environment (EURIDICE) and the Belgian
338 agency for radioactive waste management (ONDRAF/NIRAS) for their financial support.

339

340 **References**

341 ANDRA, 2005. Dossier 2005 Argile. Synthesis - Evaluation of the feasibility of a geological
342 repository in an argillaceous formation, December 2005.

- 343 Armand, G., Leveau, F., Nussbaum, C., de La Vaissiere, R., Noiret, A., Jaeggi, D., Landrein, P., and
 344 Righini, C., 2013. Geometry and Properties of the Excavation-Induced Fractures at the
 345 Meuse/Haute-Marne URL Drifts. *Rock Mechanics and Rock Engineering*, DOI:
 346 10.1007/s00603-012-0339-6.
- 347 Ashworth, T., Ashworth, E., and Ashworth, S. F., 1990. New apparatus for use with materials of
 348 intermediate conductivity, *Thermal conductivity 21* Edited by C. Cremers and A. Fine, Plenum
 349 Press, New York, 51-66.
- 350 Bastiaens, W. and Mertens, J., 2005. EDZ around an industrial excavation in Boom Clay, Proceedings
 351 of a European Commission Cluster Conference and Workshop, 305-309, C. Davies and F.
 352 Bernier (eds), Luxemburg, 3-5 November 2003, European Commission .
- 353 Beck, A.E., 1988. Methods for determining thermal conductivity and thermal diffusivity. In: Hanel,
 354 R., Rybach, L. & Stegena, L. (eds) *Handbook of Terrestrial Heat Flow Density Determination*.
 355 Kluwer, Dordrecht, 87-124.
- 356 Bernier, F., Li, X. L. and Bastiaens, W., 2007. Twenty-five years' geotechnical observation and
 357 testing in the Tertiary Boom Clay formation. *Géotechnique* (57)2, 229-237.
- 358 Brigaud, F., Chapman, D. and Le Douaran, S., 1990. Estimating thermal conductivity in sedimentary
 359 basins using lithological data and geophysical well logs. *Bulletin, American Association of*
 360 *Petroleum Geologists*, 74, 1459-1477.
- 361 Buntebarth, G., 2004. Bestimmung thermophysikalischer Eigenschaften an Opalinustonproben,
 362 Geophysikalisch-Technisches Büro, Clausthal-Zellerfeld.
- 363 Chen, G. J., Sillen, X., Verstricht, J., & Li, X. L., 2011. ATLAS III in situ heating test in Boom Clay:
 364 Field data, observation and interpretation. *Computers and Geotechnics*, 38(5), 683–696.
 365 doi:10.1016/j.compgeo.2011.04.001.
- 366 Clauser, C., and Huenges, E., 1995. Thermal Conductivity of Rocks and Minerals. In: T. J. Ahrens
 367 (ed), *Rock Physics and Phase Relations - a Handbook of Physical Constants*, AGU Reference
 368 Shelf, Vol. 3, pp. 105-126, American Geophysical Union, Washington
- 369 D5334-08, 2008. Standard Test Method for Determination of Thermal Conductivity of Soil and Soft
 370 Rock by Thermal Needle Probe Procedure.
- 371 Davies, C. and Bernier, F., 2005. Impact of the excavation disturbed or damaged zone (EDZ) on the
 372 performance of radioactive waste geological repositories. Proceedings of a European
 373 Commission Cluster Conference and Workshop, Luxemburg, 3-5 November 2003, European
 374 Commission.
- 375 Davis, M.G., Chapman, D.S., Van Wagoner, T.M., & Armstrong, P. A., 2007. Thermal conductivity
 376 anisotropy of metasedimentary and igneous rocks. *Journal of Geophysical Research*, 112(B5), 1–
 377 7. doi:10.1029/2006JB004755.
- 378 Delage, P., Le, T.-T., Cui, Y.-J., Tang, A.-M., Li, X.-L., 2007. Suction effects in deep Boom Clay
 379 block samples. *Géotechnique*, 57(2), 239–244. doi:10.1680/geot.2007.57.2.239
- 380 Farouki, O.T., 1981. Thermal Properties of Soils. Cold Region Research and Engineering Laboratory
 381 Monograph 81-1.
- 382 Farouki, O.T., 1986. Thermal properties of soils (Series in Rock and Soil Mechanics vol.11). Trans
 383 Tech Publications, Clausthal-Zellerfeld, Germany.

- 384 Gong, G., 2005. Physical properties of alpine rocks: a laboratory investigation. Thèse de doctorat:
385 Univ. Genève, no. Sc. 3658.
- 386 Grubbe, K., Haenel, R., Zoth, G., 1983. Determination of the vertical component of thermal
387 conductivity by line source methods. *Zeitblatt für Geologie und Palaontologie. Teil I H (1/2)*, 49-
388 56.
- 389 Jessop, A.M., 1990. *Thermal Geophysics*. Elsevier, Amsterdam.
- 390 Jobmann, M., Polster, M., 2007. The response of Opalinus clay due to heating: A combined analysis
391 of in situ measurements, laboratory investigations and numerical calculations. *Phys. Chem.*
392 *Earth, Parts A/B/C* 32, 929–936.
- 393 Johansen, O., 1975. *Varmeledningevne av jordarter*. Dr.ing avhandling, institutt for kjoleteknikk,
394 Norwegian Institute of Technology (NTH), Trondheim. (Thermal conductivity of soils. PhD
395 thesis, Cold Region Research and Engineering Laboratory (CRREL) Draft Translation 637,
396 1977, ADA 044002, Hanover, NH.
- 397 Mertens, J., Bastiaens, W., and Dehandschutter, B., 2004. Characterisation of induced discontinuities
398 in the Boom Clay around the underground excavations (URF, Mol, Belgium). *Applied Clay*
399 *Science*, 26(1-4), 413–428. doi:10.1016/j.clay.2003.12.017
- 400 Midttømme, K., Roaldset, E., Brantjes, J.G., 1996. Thermal conductivity of alluvial sediments from
401 the Ness Formation, Oseberg Area, North Sea. *EAGE 58th Conference, Extended Abstracts*
402 *Volume 2*, P552.
- 403 Midttømme, K., Roaldset, E., 1999. Thermal conductivity of sedimentary rocks: uncertainties in
404 measurement and modeling. *Geological Society, London, Special Publications*, 158: 45-60,
405 doi:10.1144/GSL.SP.1999.158.01.04.
- 406 Mügler, C., Filippi, M., Montarnal, P., Martinez, J.-M., Wileveau, Y., 2006. Determination of the
407 thermal conductivity of Opalinus Clay via simulations of experiments performed at the Mont
408 Terri underground laboratory. *J. Appl. Geophys.* 58, 112–129.
- 409 Munroe, R.J, and Sass J.H., 1987. Thermal conductivity of samples from borehole VC-1, Report 87-
410 184, Geological Survey.
- 411 ONDRAF/NIRAS, 2001. ONDRAF/NIRAS, SAFIR2 – Safety Assessment and Feasibility Interim
412 Report 2, ONDRAF/NIRAS report NIROND 2001-06E.
- 413 Penner, E., 1963. Anisotropic thermal conduction in clay sediments. *International Clay Conference*.
- 414 Popov, Y.A., Pribnow, D.F.C., Sass, J.H., Williams, C.F., & Burkhardt, H., 1999. Characterization of
415 rock thermal conductivity by high-resolution optical scanning. *Geothermics*, 28(2), 253–276.
416 doi:10.1016/S0375-6505(99)00007-3.
- 417 Popov, Y., Bayuk, I., Parshin, A., Miklashevskiy, D., Novikov, S., Chekhonin, E., 2012. New methods
418 and instruments for determination of reservoir thermal properties, in: *Proceedings Thirty-Seventh*
419 *Workshop on Geothermal Reservoir Engineering*. Stanford University, Stanford, California.
- 420 Popov, Y.A., 1983. Theoretical models of the method of determination of the thermal properties of
421 rocks on the basis of movable sources. *Geologiya i Razvedka (Geology and Prospecting) Part I*,
422 9, 97-103 (in Russian).

423 Pribnow, D.F.C., Davis, E.E., Fisher, A.T., 2000. Borehole heat flow along the eastern flank of the
424 Juan de Fuca Ridge, including effects of anisotropy and temperature dependence of sediment
425 thermal conductivity, Geological Survey of Canada.

426 Riche, F., and Schneebeli, M., 2012. Thermal conductivity of anisotropic snow measured by three
427 independent methods. *The Cryosphere Discussions*, 6(3), 1839–1869. doi:10.5194/tcd-6-1839-
428 2012.

429 Schön, J.H., 1996. *Physical Properties of Rocks: Fundamentals and Principles of Petrophysics*
430 Volume 18 of *Handbook of geophysical exploration: Seismic exploration*. Elsevier, Oxford.

431 Tang, A.-M., Cui, Y.-J., Le, T.-T., 2008. A study on the thermal conductivity of compacted bentonites.
432 *Applied Clay Science*, 41(3-4), 181–189. doi:10.1016/j.clay.2007.11.001.

433 Tsang C.F., Bernier F. and Davies C., 2005. Geohydromechanical processes in the EDZ in crystalline
434 rock, rock salt and indurated and plastic clays – in the context of radioactive waste disposal.
435 *International Journal of Rock Mechanics and Mining Sciences*, 42, 109-125

436 Tsang C.F., Barnichon J.D., Birkholzer J., Li X.L., Liu H.H. and Sillen X., 2012. Coupled thermo-
437 hydro-mechanical processes in the near field of a high-level radioactive waste repository in clay
438 formations. *International Journal of Rock Mechanics and Mining Sciences* 49, 31-44.

439 Yu, L., Weetjens, E. and Vietor, T., 2011. Integration of TIMODAZ Results within the Safety Case
440 and Recommendations for Repository Design. External report SCK-CEN-ER-188, SCJ-CEN,
441 Mol, Belgium.

442 Yu, L., Weetjens, E., Sillen, X., Vietor, T., Li, X.L., Delage, P., Labiouse, V., and Charlier, R., 2013.
443 Consequences of the Thermal Transient on the Evolution of the Damaged Zone Around a
444 Repository for Heat-Emitting High-Level Radioactive Waste in a Clay Formation: a Performance
445 Assessment Perspective. *Rock Mechanics and Rock Engineering*. doi:10.1007/s00603-013-0409-
446 4.

447

448

449

450

451

452

453

454

455

456

457

458

459 **List of Tables**

460 Table 1: Properties of natural Boom Clay samples taken at various distances to gallery axis (ρ_d : dry
461 density, w : water content, e : void ratio, S_r : degree of saturation) .

462 Table 2: Initial and corrected $\lambda_{//}$ values ($\lambda_{//0}$: thermal conductivity measured on non-saturated samples,
463 Corrected $\lambda_{//}$: saturated thermal conductivity after Johansen's method, $\Delta\lambda_{//}$: difference between the
464 $\lambda_{//0}$ and Corrected $\lambda_{//}$).

465

466 **List of Figures**

467 Fig.1: Principal axes of thermal conductivity for the three cases studied with the needle probe method.
468 A, B and C: main (orthogonal) axes of thermal conductivity (A is perpendicular to the bedding plane;
469 B and C are parallel to the bedding plane).

470 Fig.2: Running a test by the needle probe method (a): system for drilling; (b) inserting the needle
471 probe into the specimen with marks of the bedding plane.

472 Fig.3: Measurement of thermal conductivity.

473 Fig.4: Thermal conductivity versus distance r to the axis of the gallery.

474 Fig.5: Degree of thermal conductivity anisotropy versus distance r to the axis of the gallery.

475

476

477 Table 1: Properties of natural Boom Clay samples taken at various distances r to gallery axis (ρ_d : dry
478 density, w : water content, e : void ratio, S_r : degree of saturation)

Test	Distance r (m)	ρ_d (kg/m ³)	w (%)	e	S_r (%)
TH6	2.5	1610	23.98	0.65	97.9
TH7	2.6	1640	23.05	0.63	98.0
TH8	2.7	1640	23.05	0.63	98.0
TH14	3.4	1630	23.51	0.64	98.4
TH13	3.8	1630	23.02	0.63	98.0
TH12	6.0	1630	22.84	0.64	95.2
TH11	9.2	1640	22.63	0.63	96.3
TH10	16.0	1640	22.61	0.63	96.2
TH9	20.8	1630	23.48	0.64	98.4

479

480

481

482

483 Table 2: Initial and corrected $\lambda_{//}$ values ($\lambda_{//0}$: thermal conductivity measured on non-saturated samples,
484 Corrected $\lambda_{//}$: saturated thermal conductivity after Johansen's method, $\Delta\lambda_{//}$: difference between the
485 $\lambda_{//0}$ and Corrected $\lambda_{//}$).

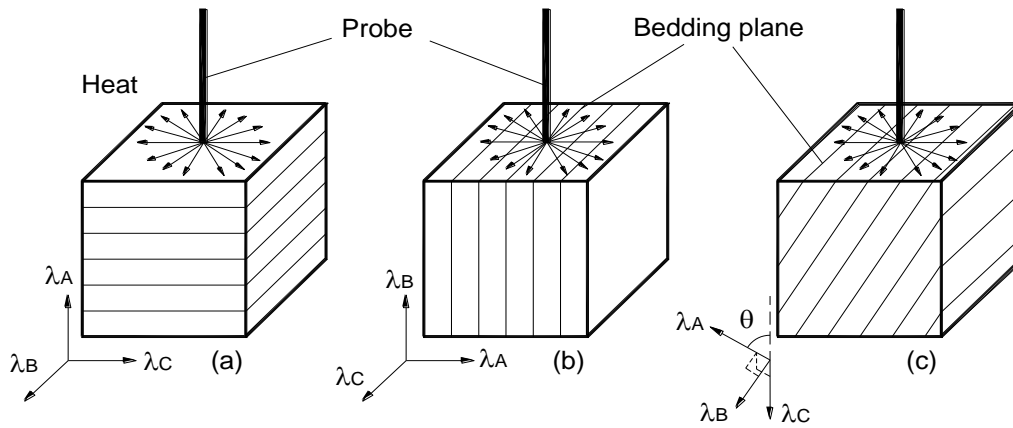
Tests	Distance r (m)	S_r	$\lambda_{//0}$ (W/(m.K))	Corrected $\lambda_{//}$ (W/(m.K))	$\Delta\lambda_{//} / \lambda_{//(\text{measured})}$ (%)
TH6	2.5	97.9	1.33	1.34	0.85
TH7	2.6	98.0	1.38	1.39	0.80
TH8	2.7	98.0	1.41	1.42	0.80
TH14	3.4	98.4	1.45	1.46	0.64
TH13	3.8	98.0	1.54	1.55	0.81
TH12	6.0	95.2	1.56	1.59	2.04
TH11	9.2	96.3	1.58	1.61	1.55
TH10	16.0	96.2	1.49	1.51	1.57
TH9	20.8	98.4	1.52	1.53	0.67

486

487

488

489



490

491 Fig. 1: Principal axes of thermal conductivity for the three cases studied with the needle probe method.

492 A, B and C: main (orthogonal) axes of thermal conductivity (A is perpendicular to the bedding plane;

493 B and C are parallel to the bedding plane).

494



495

496

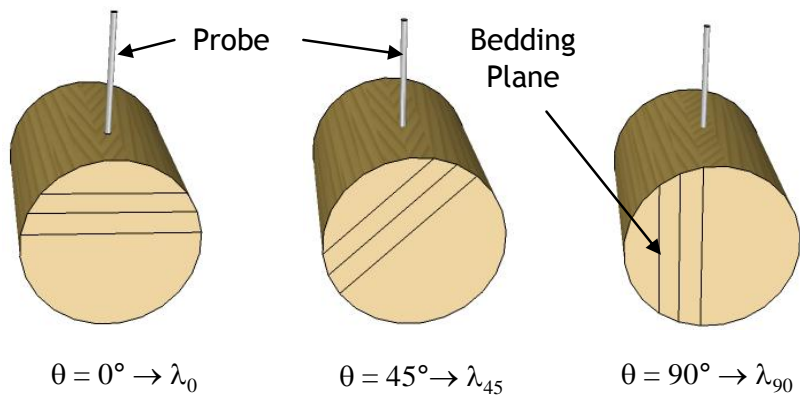
(a)

(b)

497 Fig. 2 : Running a test by the needle probe method (a): system for drilling; (b) inserting the needle

498 probe into the specimen with marks of the bedding plane.

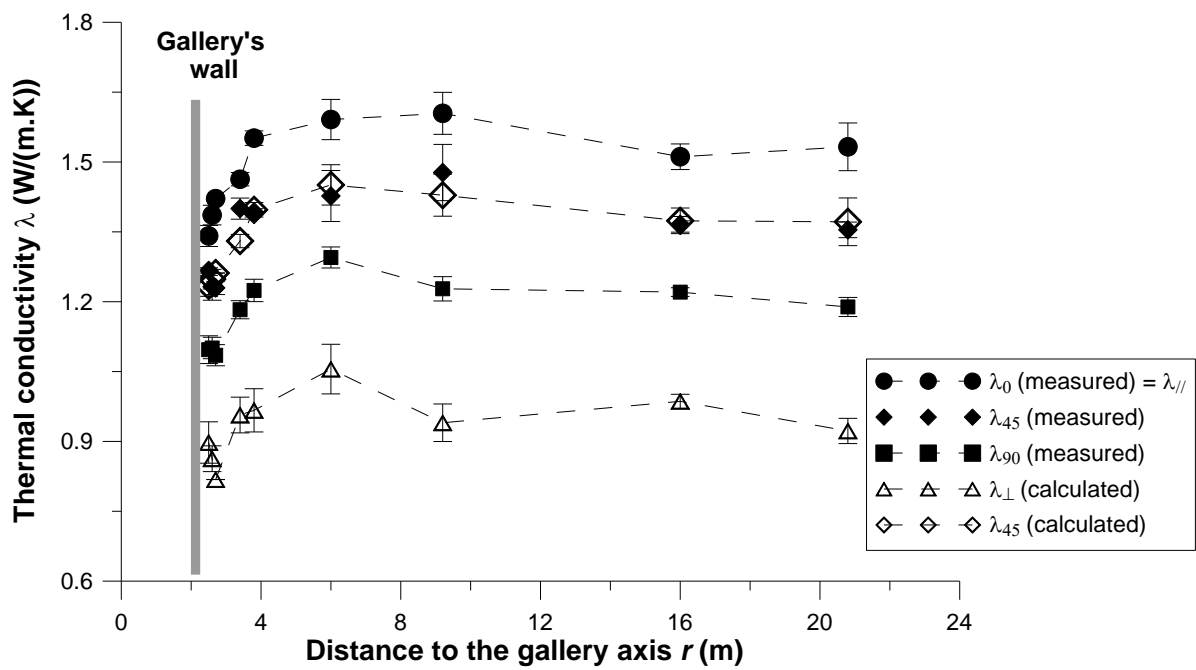
499



500

501 Fig. 3 : Measurement of thermal conductivity.

502



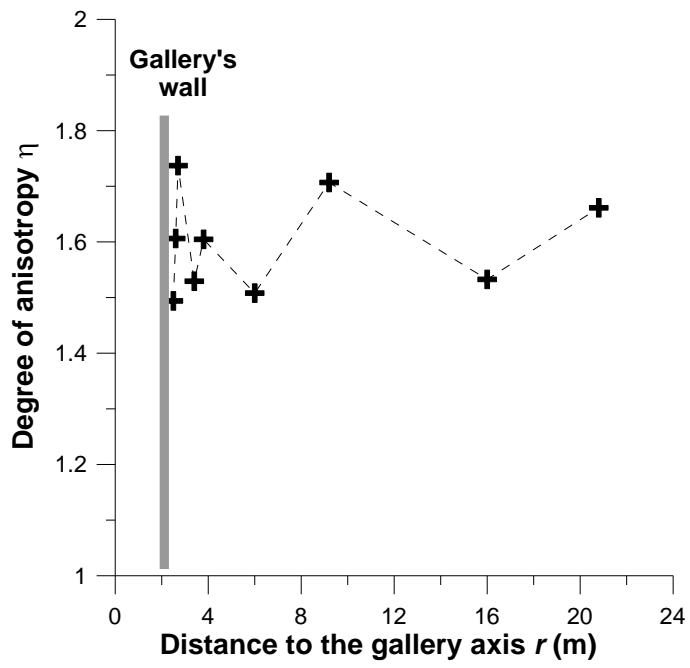
503

504 Fig. 4: Thermal conductivity versus distance r to the axis of the gallery.

505

506

507



508

509 Fig. 5: Degree of thermal conductivity anisotropy versus distance r to the axis of the gallery.

510

511

512